E. S. Cross
Department of Civil and Environmental Engineering, Massachusetts Institute of Technology, Cambridge, MA 02139

A. Sappok
Sloan Automotive Laboratory, Massachusetts Institute of Technology, Cambridge, MA 02139

E. C. Fortner
Center for Aerosol and Cloud Chemistry, Aerodyne Research Inc., Billerica, MA 01821

J. F. Hunter
Department of Civil and Environmental Engineering, Massachusetts Institute of Technology, Cambridge, MA 02139

J. T. Jayne

W. A. Brooks

T. B. Onasch

Center for Aerosol and Cloud Chemistry, Aerodyne Research Inc., Billerica, MA 01821

V. W. Wong
Sloan Automotive Laboratory, Massachusetts Institute of Technology, Cambridge, MA 02139

A. Trimborn
Center for Aerosol and Cloud Chemistry, Aerodyne Research Inc., Billerica, MA 01821; AeroMegt GmbH, Hilden 40723, Germany

D. R. Worsnop
Center for Aerosol and Cloud Chemistry, Aerodyne Research Inc., Billerica, MA 01821

J. H. Kroll
Department of Civil and Environmental Engineering, Massachusetts Institute of Technology, Cambridge, MA 02139; Department of Chemical Engineering, Massachusetts Institute of Technology, Cambridge, MA 02139

Real-Time Measurements of Engine-Out Trace Elements: Application of a Novel Soot Particle Aerosol Mass Spectrometer for Emissions Characterization

Lubricant-derived trace element emissions are the largest contributors to the accumulation of incombustible ash in diesel particulate filters (DPF), eventually leading to filter plugging and an increase in engine fuel consumption. Particulate trace element emissions also pose adverse health effects and are the focus of increasingly stringent air quality regulations. To date, the rates and physical and chemical properties of lubricant-derived additive emissions are not well characterized, largely due to the difficulties associated with conducting the measurements. This work investigated the potential for conducting real-time measurements of lubricant-derived particle emissions. The experiment used the Soot Particle Aerosol Mass Spectrometer (SP-AMS) developed by Aerodyne Research to measure the size, mass and composition of submicron particles in the exhaust. Results confirm the ability of the SP-AMS to measure engine-out emissions of calcium, zinc, magnesium, phosphorous, and sulfur. Further, emissions of previously difficult to detect elements, such as boron, and low-level engine wear metals, such as lead, were also measured. This paper provides an overview of the results obtained with the SP-AMS, and demonstrates the utility of applying real-time techniques to engine-out and tailpipe-out trace element emissions. Application of the SP-AMS for engine exhaust characterization followed a two-part approach: (1) measurement validation, and (2) measurement of engine-out exhaust. Measurement validation utilized a diesel burner with precise control of lubricant consumption. Results showed a good correlation between CJ-4 oil consumption and measured levels of lubricant-derived trace elements in the particle phase. Following measurement validation, the SP-AMS measured engine-out emissions from a medium-duty diesel engine, operated over a standard speed/load matrix. This work demonstrates the utility of state-of-the-art online techniques (such as the SP-AMS) to measure engine-out emissions, including trace species derived from lubricant additives. Results help optimize the combined engine-lubricant-aftertreatment system and provide a real-time characterization of emissions. As regulations become more stringent and emission controls more complex, advanced measurement techniques with high sensitivity and fast time response will become an increasingly important part of engine characterization studies. [DOI: 10.1115/1.4005992]

1 Introduction

Increasingly stringent regulations have necessitated the development and widespread introduction of advanced aftertreatment technologies, such as diesel particulate filters (DPF) [1], to decrease particle emissions below regulated levels. While extremely effective at trapping engine-out particulate matter (PM)

Contributed by the IC Engine Division of ASME for publication in the JOURNAL OF ENGINEERING FOR GAS TURBINES AND POWER. Manuscript received October 18, 2011; final manuscript received October 22, 2011; published online May 23, 2012. Editor: Dilip R. Ballal.

emissions (reducing tailpipe PM mass emissions by ~99% in some cases), ash also accumulates in the DPF over time. Unlike the PM which can be oxidized and effectively removed from the DPF during filter regeneration, the incombustible ash remains and builds-up over multiple regeneration cycles. Ash accumulation restricts exhaust flow through the DPF, increases engine backpressure, and incurs an additional fuel consumption penalty. Ultimately the build-up of ash in the DPF determines the filter's service life. DPF ash originates primarily from metallic additives in the engine lubricating oil, predominately calcium (Ca), zinc (Zn) and magnesium (Mg), which are found in the DPF as various metallic-oxides, sulfates and phosphates [2]. These lubricant-derived metallic particles (ash precursors) are generally transported to the DPF through the exhaust bound to the carbonaceous particulate matter [3]. While most of the PM and associated ash-related elements are trapped on the DPF, there is also increasing concern related to nano-size metal emissions from diesel engines, and in particular from gasoline engines not equipped with DPFs [4].

A consequence of increasingly stringent emission standards is a corresponding requirement for advanced emission characterization methods with low detection limits, fast time response and high sensitivity to the regulated species of interest [5]. The field of aerosol mass spectrometry has grown significantly over the past 20 years and has resulted in the development of quantitative, online measurements of the size, mass and chemical composition of submicron particulate matter. In general, two types of aerosol mass spectrometry platforms exist: single particle measurement techniques that utilize laser ablation/ionization [6] and ensemble average techniques based on thermal desorption and electron impact ionization [7]. Single particle mass spectrometers such as the Aerosol Time-of-Flight Mass Spectrometer (ATOFMS) have been used to characterize the size and chemical composition of individual particles emitted by combustion engines as a function of engine operation [8–10]. In those studies, the contribution of lubricating oil additives to the emitted PM was inferred from calcium and phosphate peaks in the single particle mass spectra. Thermal desorption/electron impact ionization methods such as the Aerosol Mass Spectrometer (AMS) offer the advantage of quantification of the nonrefractory species (those that readily vaporize at 600 °C) but provide no chemical information about the refractory components of the particles in the traditional configuration of the instrument [11,12].

The work presented here demonstrates the use of a newly developed version of the AMS called the Soot Particle Aerosol Mass Spectrometer or SP-AMS. The SP-AMS, developed by Aerodyne Research, Inc., uses a continuous intra-cavity 1064 nm laser beam to vaporize refractory particles. The continuous laser vaporization source differentiates the SP-AMS technique from laser ablation/ionization instruments which use a pulsed, high energy laser to ablate and ionize the particles. A detailed description of the SP-AMS instrument and its application is found in the literature [13]. Briefly, particles sampled by the SP-AMS that contain constituents that absorb 1064 nm light will heat up and vaporize as they intersect the laser beam. The resulting vapor molecules are ionized via electron impact and analyzed with high resolution mass spectrometry. The SP-AMS used in this study is also equipped with a conical vaporizer (the nominal vaporization method for all AMS instruments). Therefore, whether the intra-cavity laser beam is on or off, the nonrefractory constituents in the particles are vaporized, ionized and detected. Results from engine-lab tests are presented with a focus on demonstrating the capability of the SP-AMS for in situ ash characterization in the exhaust PM.

2 Experimental Setup and Procedures

Experiments were conducted following a two-stage approach, utilizing two different combustion sources: (I) instrument validation, using an accelerated ash loading system comprised of an industrial diesel burner coupled to a combustion chamber and (II) engine exhaust characterization, using a Cummins development engine based on the 2002 ISB 300 platform. Both sources, and the emissions testbed used, have been described in detail in previous publications [3,14]. The specifications for the engine and burner are outlined in Table 1 and Table 2, respectively. A schematic of the experimental setup is shown in the Appendix.

Table 1 Cummins 2002 ISB 300 engine specifications

Engine parameter	Description
Model	ISB 300
Maximum torque	890 N m at1600 RPM
Maximum power	224 kW at 2500 RPM
Number of cylinders	In-line 6
Combustion system	4-stroke, direct injection
Injection system	Common rail
Aspiration	Variable geometry turbocharger and intercooler
Displaced volume	5.9 L
Compression ratio	17.2:1
Cylinder head layout	4 valves/cylinder
Injection nozzle	O.D. = 158 um, L = 1.00 mm, 8 sac-less nozzles/injector
Injection pressure	800-1600 bar

Table 2 Specifications of the accelerated ash loading system

System parameter	Description
Fuel consumption	1.5–7.6 L/hour
Oil consumption	0.94–9.4 mL/min
Injection pressure	700–1400 kPa
Air flow	266–1130 sLpm
DPF inlet temperature	200-800 °C

The combustion chamber is equipped with a computer-controlled oil injector system for precise addition of lubricant. As shown in Figure A1, a heat-exchanger is mounted downstream of the burner system to provide additional control over exhaust temperature. During the instrument validation experiments, the exhaust temperature was maintained at approximately 300 °C.

2.1 Previous Work. Previous studies comparing burner- and engine-generated PM showed no significant differences, aside from elevated ash concentration and slightly larger diameter particles (factor of 2) produced by the burner system [15]. Offline analyses of laboratory- and field-loaded DPFs also reported similar ash composition, packing density and distribution in both cases [16]. These results validate the use of the accelerated ash loading system for characterizing the instrument response to lubricant-derived ash emissions. The accelerated ash loading system was used during the validation experiments because of the precise control and wider range of oil consumption conditions possible relative to the engine platform.

2.2 Sampling Inlet. For the results presented here, the particle sampling inlet was positioned on the engine side of the DPF (Position 'A' shown in Figure A1). The particle inlet had primary and secondary dilution stages. The first dilution stage consisted of a mini-eductor (Fox Valve Development Corp.) with dilution factors ranging from 2–4 depending on the backing pressure of nitrogen gas applied and the resultant suction flow at the inlet tip (1.5–2.5 L/min). The inlet tip was positioned at the centerline of the exhaust sampling pipe approximately 6 inches (15.24 cm) upstream of the DPF. The secondary dilution stage consisted of a stainless steel chamber (3L) allowing for additional dilution (nitrogen with a mass flow controller), pressure equalization and mixing. Prior to sampling with the SMPS and SP-AMS systems the flow was directed through a 36 in (91.44 cm) long diffusion dryer to minimize water interference in the SP-AMS.

Table 3 Lubricant elemental composition

	ASTM D5185							
Lubricant	B (ppm)	Ca (ppm)	Fe (ppm)	Mg (ppm)	P (ppm)	Zn (ppm)	S (ppm)	Mo (ppm)
CJ-4	586	1388	2	355	985	1226	3200[a]	77

[a]Value supplied by manufacturer.

Table 4 Fuel elemental composition. All values below minimum detectable limits.

	ASTM D5185					
Fuel	Ca (ppb)	Mg (ppb)	P (ppb)	Na (ppb)	K (ppb)	Zn (ppb)
ULSD	< 97	< 56	< 1180	< 2010	< 2690	< 155

2.3 Instrumentation. Two instruments were used to characterize the physical and chemical properties of the engine exhaust particles: a Scanning Mobility Particle Sizer (SMPS) (from TSI, Inc.) and the SP-AMS. For the second phase of validation experiments, a Differential Mobility Analyzer (DMA) was also used to size-select the particle distributions prior to sampling with the SMPS and SP-AMS.

The AMS has been described extensively in the literature (for a recent review see Ref. [7]). A detailed characterization of the SP-AMS used in this study is presented by Onasch et al. [13]. Briefly, the instrument operation is similar to the traditional AMS configuration with the exception of the 1064 nm intra-cavity laser vaporization source. Following vaporization (either by impact with the conical 600 °C vaporizer surface or within the intra-cavity 1064 nm laser) vapor molecules are ionized via electron impact (EI) ionization and detection via a high resolution time-of-flight mass spectrometer (HR-TOFMS). One of the key strengths of the SP-AMS is the electron impact (EI) ionization source. EI results in a total ion count at the detector that is proportional to the total mass of vapor molecules formed. The traditional configuration of the AMS has shown that EI-high resolution mass spectrometry provides quantitative chemical composition information for ambient aerosol particles composed of nonrefractory constituents [7]. The SP-AMS used here offers a unique opportunity to explore the potential of the EI-HR-TOFMS technique for identification and quantification of refractory components in the exhaust that strongly absorb at 1064 nm. The results obtained in this study offer the first insights into how well lubricant-derived metal species are measured with this new instrument configuration.

2.4 Data Acquisition (DAQ). The DAQ program for the SP-AMS allows the user to sample from different data collection menus over the course of an experiment to maximize the chemical and physical information obtained with the instrument. In this study, the SP-AMS data were collected continuously and averaged over 60 s time intervals. During each 60 s 'run' the instrument toggled between particle time-of-flight (PToF) mode and mass spec (MS) mode with a 50% duty cycle in each. In PToF mode, the vacuum aerodynamic diameter of the particle ensemble is determined by using a chopper to modulate the particle beam as it enters the vacuum chamber. In MS mode, the particle beam is alternately opened and blocked and a complete mass spectrum is measured in both instances. The instrument background (or closed spectrum) is then subtracted from the open spectrum to give the difference mass spectrum attributed to the particle ensemble. As this work is primarily focused on understanding the chemical (rather than physical) properties of the particles, The data presented in this manuscript are all obtained during MS mode only.

The SP-AMS used in this experiment sampled alternate runs with the intracavity 1064 nm laser turned ON/OFF to allow for comparison of the mass spectra measured with and without the laser vaporization source. With the laser turned off, the instrument is configured as a traditional AMS, with the conical 600 °C vaporizer as the only means for vaporizing the particles. The expectation is that with the laser turned OFF, lower-volatility (refractory) components within the particles will not be vaporized or detected. For the results presented here, the intracavity laser was turned on at all times.

The HR-TOFMS has two ion path length settings denoted 'W' mode and 'V' mode [12]. In 'W' mode the ion transmit path length is longer resulting in higher mass resolution ($\sim$5000 up to $m/z = 200$) but lower ion throughput to the detector (lower sensitivity). The relatively shorter ion path length in 'V' mode results in a mass resolution of $\sim$2100 (up to $m/z = 200$) and greater ion throughput (higher sensitivity). The results presented here were all obtained with the SP-AMS in V mode. The SMPS was set to scan every 120 s throughout the experiment. The sheath flow to aerosol flow was held at 10:1 with the exception of the validation experiment discussed in Sec. 3.3.

2.5 Test Matrix and Procedures. The lubricant used in this study was a SAE 15W-40 commercially available CJ-4 diesel engine oil. Table 3 lists the elemental composition of the CJ-4 oil [14]. The Cummins ISB and burner system were fueled with ultra-low sulfur diesel (ULSD, 15 ppm S). The elemental composition of the ULSD is shown in Table 4 [14].

During the instrument validation phase of the experiment, the diesel burner/oil injector system was used to produce stable distributions of combustion particles formed via careful control of the CJ-4 oil injection rates. Two validation experiments were conducted. In the first experiment, the oil injection rate was systematically increased and the polydisperse distribution of combustion particles was sampled with the SP-AMS and SMPS systems. In the second experiment, the oil injection rate was held constant and the DMA was used to size-select $d_m \sim 100$ nm particles prior to sampling with the SP-AMS and SMPS systems. In this set of experiments, the mass concentration was controlled by varying the sheath flow rate in the DMA.

The objective of the first validation experiment was to determine if the SP-AMS could detect lubricant-derived metal species under conditions characterized by extreme, and known, oil consumption simulated with the accelerated ash loading system. The objective of the second series of validation experiments was to determine if the ion response of the SP-AMS was linear with total particle mass.

Following system validation using the accelerated ash loading burner, the SP-AMS was used to characterize particulate ash species from real diesel engine exhaust. In these tests, the Cummins ISB engine was used as the source and emission profiles were measured across a range of engine speed and load conditions. The primary objective of these initial engine experiments was to determine the ability of the SP-AMS to positively identify the low-level additive-related emissions in actual engine exhaust at a qualitative level. Subsequent studies will focus on developing quantitative calibrations based on the results of this feasibility study.

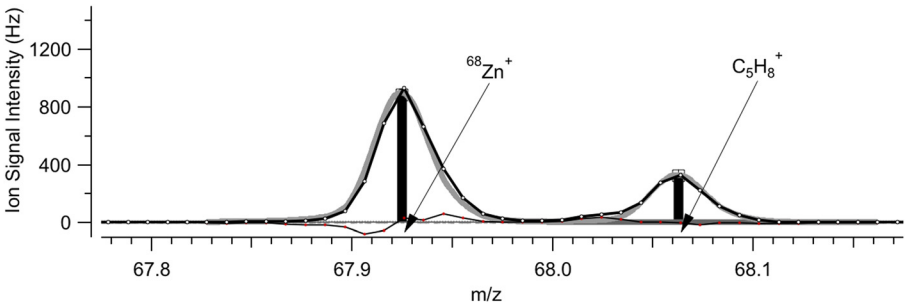

Fig. 1 Ion signal intensities measured at nominal m/z = 68 showing a peak corresponding to the Zn_{68}^{+} isotope at 67.9248 amu and a hydrocarbon fragment $C_5H_8^{+}$ at 68.0626 amu. The residual between the peak fit and raw data is also plotted in the figure.

3 Results and Discussion

3.1 Resolving Power. To demonstrate the mass resolving power ($m/\Delta m$) of the SP-AMS, Fig. 1 provides an example showing a mass-to-charge (m/z) ratio of 68 for two peaks within +/− 0.1 amu of one another. The peak separation demonstrated in Fig. 1 shows that the SP-AMS (operating in 'V' mode) can unambiguously and simultaneously identify metallic and hydrocarbon ion fragments at the same nominal m/z. The SP-AMS data were processed using the fitting algorithms in the SQUIRREL (Sequential Igor Data Retrieval, version 1.50) and PIKA (Peak Integration by Key Analysis version 1.09) software toolkits.

3.2 Isotopic Abundance. Trace elements found in engine exhaust, such as zinc, boron, magnesium, potassium and sulfur have naturally occurring, stable isotopes. Isotope signatures provide a framework for confirming the accuracy of the SP-AMS mass calibration and peak integration procedures. Figures 2 and 3 plot the parent and isotope ion signals for zinc and boron against the total ion signal measured for each species. The slope of each line corresponds to the empirically measured isotopic abundance. The data shown in Figs. 2 and 3 span the full range of CJ-4 oil injection rates tested in the first phase of the validation experiments. The slope (*i.e.* isotopic abundance) determined with each linear fit is shown in the legend. In the case of each stable isotope of zinc and the stable isotope for boron, the measured abundance is within 3% of the literature value [17].

3.3 Validation Experiments I: Measurements as a Function of Oil Injection Rate. Figure 4 displays time series of the ion signal intensities for boron (Σ B_{10}, B_{11}), sodium, calcium, phosphorus, sulfur, potassium, calcium and zinc (Σ Zn_{64}, Zn_{66}, Zn_{67}, Zn_{68}) during a period of increasing CJ-4 oil injection using the accelerated ash loading system. The lower panel of Fig. 4 shows an image plot of the SMPS size distribution (based on the particle number concentration). The ion signal intensities are plotted on separate y-axes to encompass the large dynamic range of ion signals for different ash species. The shaded gray region of the plot displays the CJ-4 oil injection rate: 0, 0.8, 1.6, 3.2, 4 and 6.4 mL/min during this validation experiment. The SP-AMS measurements clearly show increasing boron, phosphorus, sodium, sulfur, potassium and zinc with increasing oil injection rate. This observation is consistent with the fact that the CJ-4 oil is the main source of these metallic species. The calcium ion signals follow a different trend. Calcium ion signals peak at an injection of 3.2 mL/min and decline with higher injection rates. Currently, the reason for this declining trend is unclear; however, it is possible that some of the calcium may be preferentially deposited inside the burner/exhaust sampling system or instrument. Nonetheless, the relative proportion of the Ca and Zn ion intensities at the oil injection rate of 3.2 mL/min is roughly consistent with their proportion in the lubricating oil.

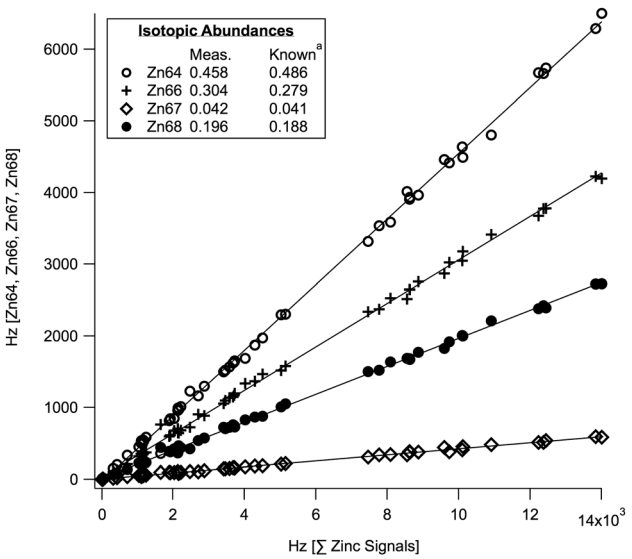

Fig. 2 Empirical measurement of the isotopic abundance for each major isotope of zinc

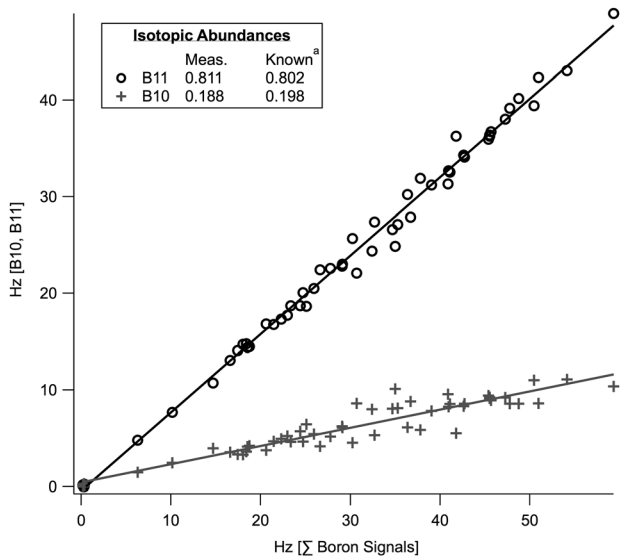

Fig. 3 Empirical measurement of isotopic abundance for boron

3.4 Validation Experiments II: Linear Ion Response. In the second phase of the validation experiments, the accelerated ash-loading system was operated at a constant oil injection rate of 2.4 mL/min. The objective of this test was two-fold: to determine if the integrated ion signals for ash-species scale linearly with

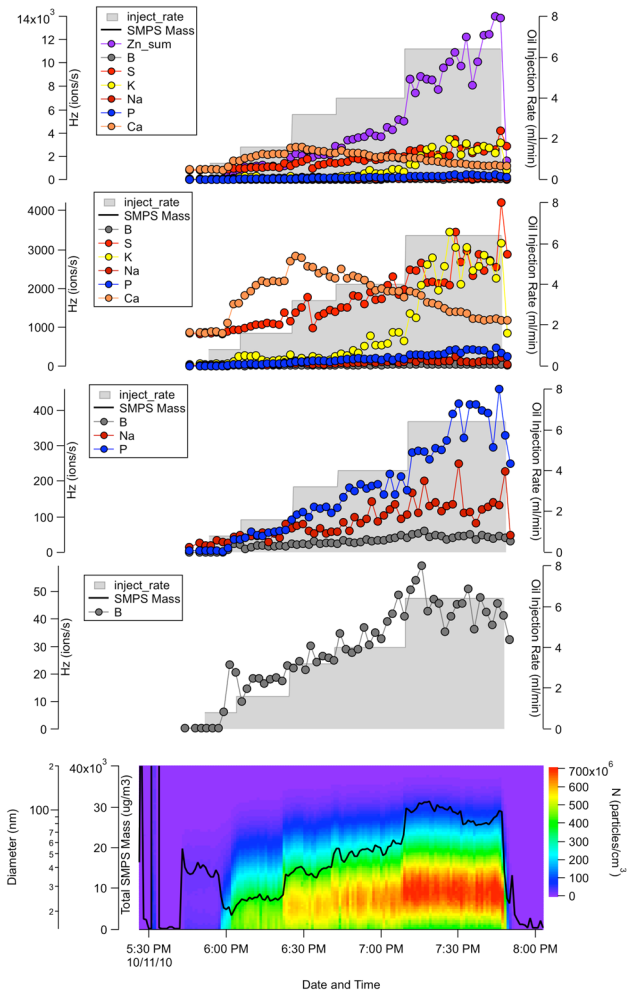

Fig. 4 Specific lubricant-derived ash species ion signal intensities as a function of increasing CJ-4 oil injection rate. SMPS-measured size distribution is displayed as an image plot colored by the number concentration in the lower panel of the plot.

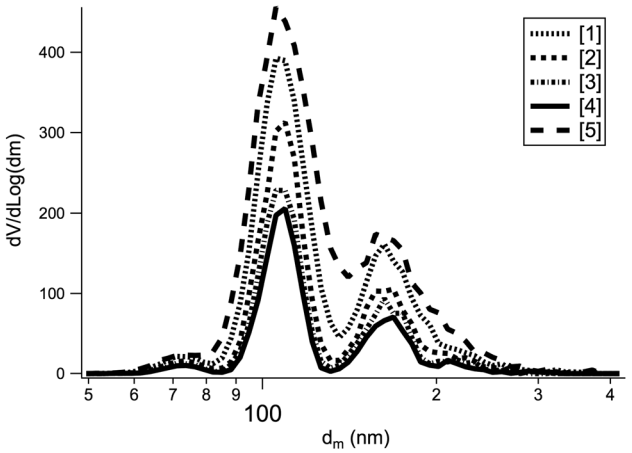

Fig. 5 SMPS volume distributions obtained by varying the sheath flow rate in the size-selecting DMA to systematically control the total mass concentration of particles sampled with the SP-AMS. The bi-modal distribution results from doubly charged particles (with equivalent mobility to singly charge 100 nm particles) being transmitted through the size-selecting DMA.

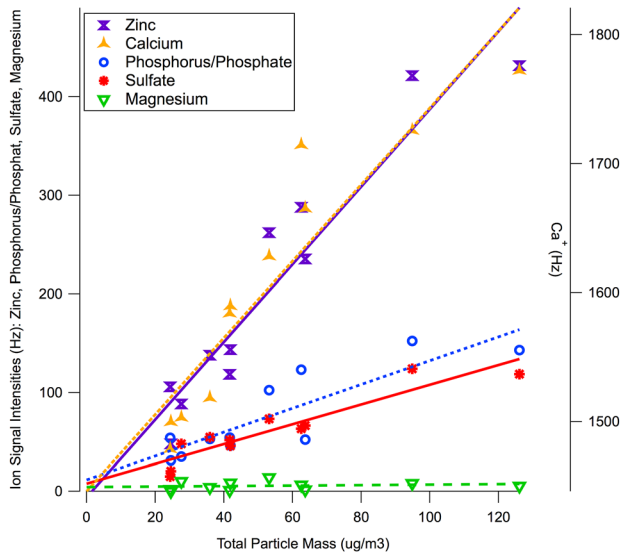

Fig. 6 Ion response for calcium, zinc, phosphorus and sulfate species as a function of total particle mass measured with the SMPS

total particle mass, and provide the basis for the quantification and mass closure analysis.

A DMA was used to size-select $d_m \sim 100$ nm particles prior to sampling with the SP-AMS and SMPS to ensure all particles were of a size that they would be fully transmitted to the SP-AMS detection region [18]. The mass concentration was systematically varied by changing the sheath air flow rate in the DMA to progressively broaden the particle distribution transmitted to the instruments. The SMPS distribution for each mass concentration tested is shown in Fig. 5.

For each volume concentration shown in Fig. 5, the zinc, calcium, magnesium, phosphorus/phosphate, and sulfate ion signals were obtained with the SP-AMS. Figure 6 displays the ash signal intensities as a function of the total mass concentration, calculated from the SMPS distributions shown in Fig. 5 (assuming spherical particles with a density of 1 g/cm^3).

The data in Fig. 6 were fit with linear regressions and the slope, intercept and R^2 values of each fit are listed in Table 5. For all ash-species except magnesium, the data are well represented with linear fits ($R^2 > 0.85$). The magnesium signals are below the detection limit for this accelerated ash condition. One should note that the calcium ion signals are plotted on the right-hand axis and have a large positive offset in the y-intercept of the linear fit. This intercept is likely due to higher Ca^+ ion background signals in the SP-AMS that lead to a nonzero baseline. Additional analysis is underway to understand the origin of this Ca^+ background.

The ultimate goal when applying quantitative online measurement techniques to emissions characterization is to directly measure all gas and particle emissions as a function of the fuel consumption/engine operating conditions. Toward this goal, in Fig. 7 we present measured mass loadings in μg/m^3 for zinc, phosphorus/phosphate and calcium as a function of the calculated mass concentration of each species. The calculated concentrations (displayed on the x-axis) were derived from the oil injection rate, oil density, whole oil elemental composition (shown in Table 3) burner air flow rate and sampling line dilution. This is an upper limit to the loading that may be present in the particles, since it assumes that all of the additive material in the CJ-4 is in the particle phase and no losses are incurred along surfaces located between the burner and the SP-AMS inlet. The measured mass concentrations (displayed on the y axis) are obtained by assuming the sensitivity of the SP-AMS towards these additive-derived components is equal to that of ammonium nitrate. This assumes these species have the same ionization efficiency as ammonium nitrate [19], and the particles are measured with a collection efficiency of 1 (all particles entering the detection region are measured).

The data shown in Fig. 7 indicate that ~0.5% of the calculated zinc and calcium and ~0.25% of the calculated phosphorus/

Table 5 Fit Coefficients for the linear regressions shown in Fig. 6

Species	Slope	Y-intercept	R^2
Zinc	3.94	−6.14	0.95
Calcium	2.97	1446	0.93
Phosphorus/phosphate	1.21	11.5	0.86
Sulfate	1.00	7.58	0.93
Magnesium	0.02	4.22	0.18

phosphate is measured with the SP-AMS. The difference between measured and calculated mass loadings can be attributed to experimental uncertainties in the SP-AMS parameterization as well as exhaust line losses. To improve the interpretation of the results, the SP-AMS CE and IE factors must be empirically determined for the specific lubricant additive-derived species of interest. If the ash particles within the exhaust PM are not bound to carbonaceous particles, the particles will not strongly absorb the 1064 nm laser light and detection efficiency will decrease. Losses due to surfaces within the exhaust sampling system and volatile species that remain in the gas phase need be quantified for reliable calculations of the expected mass concentration at the instrument inlet.

To improve the accuracy of the mass closure analysis, off-line analysis techniques will be used in future experiments to better quantify the mass fraction of particulate species at the downstream sampling inlet position of the SP-AMS. With this information, particle loss to the exhaust line surfaces and species entrained in the gas phase will be excluded from the calculated mass. Additionally, species-specific ionization efficiency curves for the modified SP-AMS will be derived to determine if the SP-AMS response is well characterized with a single value across all ash-species or if unique calibration curves are required. The linear fits shown in Fig. 6 are the first step toward assessing the potential of the SP-AMS to provide a quantitative measure of the mass loading of ash-species.

3.5 Engine Exhaust Characterization. The results discussed in Secs. 3.1–3.4 indicate that the SP-AMS instrument can measure lubricant-derived-species of interest and that the ion signal intensity for measured species scales linearly with total particle mass. The next series of experiments evaluated the SP-AMS measurement capability in the context of engine emissions across a range

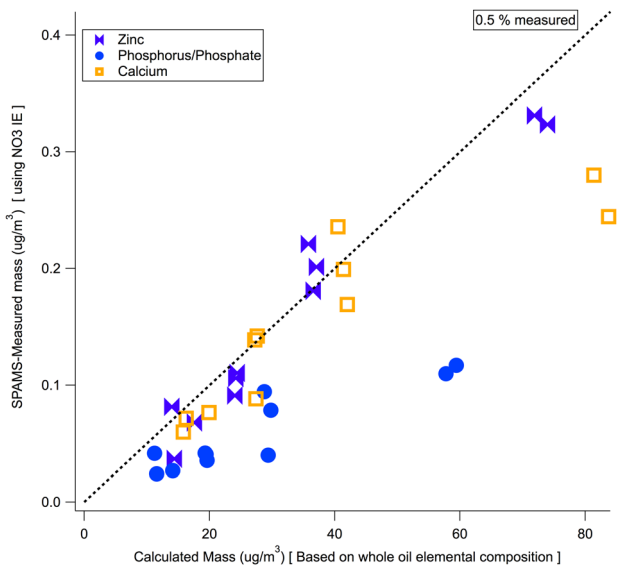

Fig. 7 SP-AMS measured mass concentrations for zinc, calcium and phosphorus/phosphate as a function of calculated mass concentrations for each component based on elemental analysis of CJ-4

of speed and load operating conditions. All engine-out SP-AMS results are reported in Hz. Future studies will focus on characterizing species-specific ionization efficiencies of the instrument.

3.5.1 Data Considerations. As stated in Sec. 2.2, all measurements presented in this paper were taken at sampling position A (See Figure A1) approximately 6 inches (15.24 cm) upstream of the DPF. A mini-eductor and secondary dilution chamber were used to adjust the particle concentration measured with the SP-AMS and SMPS during the tests. To account for changes in dilution, the SP-AMS ion signals are normalize to the total SMPS mass. While the data presented in this feasibility study covers only a small subset of the engine's speed and load map, future work will expand the number of engine operating conditions.

For the sake of clarity and to fully capture the range of speed and load conditions tested, all graphs in the subsequent sections displaying engine emission data are constructed with the same organizational scheme. Briefly, marker type denotes chemical species, marker color corresponds to engine speed, and marker size is proportional to engine load. To facilitate comparison of the data, the horizontal axis in each figure is the mass-normalized zinc signal. The zinc ion signals were chosen as the common metric because zinc was reliably measured for all engine operating conditions and allows for qualitative comparisons between lubricant-derived emissions and other engine/fuel-derived emissions.

3.5.2 Lubricant-Derived Metal Species. The elemental composition of the CJ-4 oil used in this study was shown in Table 3. The additive formulation contains predominately sulfur, calcium, zinc and phosphorus. The composition of the ash that accumulates in the DPF is likewise dominated by these elements. The SP-AMS offers the ability to monitor, in real-time, relative changes in particulate species in the exhaust stream as a function of engine operation. Figures 8(*a*) and 8(*b*) summarize the SP-AMS measurements of calcium, phosphorus/phosphate, zinc, sulfate and magnesium across the full range of engine speed and load conditions studied.

The overall trends in Figs. 8(*a*) and 8(*b*) show increased ash signal intensity with engine operating conditions consistent with increasing bulk oil consumption. Generally, total engine oil consumption is observed to increase with increasing engine speed and load [20,21]. Figures 8(*a*) and 8(*b*) show a clear increase in lubricant-derived trace element emission rates with increasing engine load from 220 Nm to 630 Nm for both the low and high engine speed conditions.

On the other hand, the effect of increased engine speed on the elemental emission rates is less obvious. Insights can be made by focusing on the elemental emissions at a constant load of 220 Nm (the smallest symbol size on each graph). At this load, the signal intensities for calcium, phosphorus/phosphate, sulfate, magnesium and zinc all increase when the engine speed increases from 1700 to 2100 RPM (red to green color transition). However, further increasing the engine speed from 2100 to 2450 RPM (green to purple color transition) did not appreciably change the calcium, sulfate and zinc signals and caused a slight decrease in the magnesium and phosphorus/phosphate levels.

Studies have shown differences in lubricant-derived elemental emissions rates due to differences in the volatilities of the specific additive constituents. In particular, zinc and phosphorous are generally emitted at higher rates, due to their higher volatility, than calcium and magnesium, which are preferentially concentrated in the oil sump [22]. Differences in additive volatility should have a larger effect on volatile lubricant-additive loss mechanisms and little effect on liquid losses, which are primarily due to bulk oil transport in the power cylinder. As engine load is increased, in-cylinder temperatures also increase quite substantiality, leading to a relative increase in the volatile oil consumption mechanism. On the other hand, as engine speed increases, liquid oil transport becomes an increasingly important oil consumption mechanism relative to volatile losses [23]. The preferential retention of calcium and magnesium in the oil sump, and higher volatility of zinc dialkyldithiophosphates (ZDDP), particularly in the high

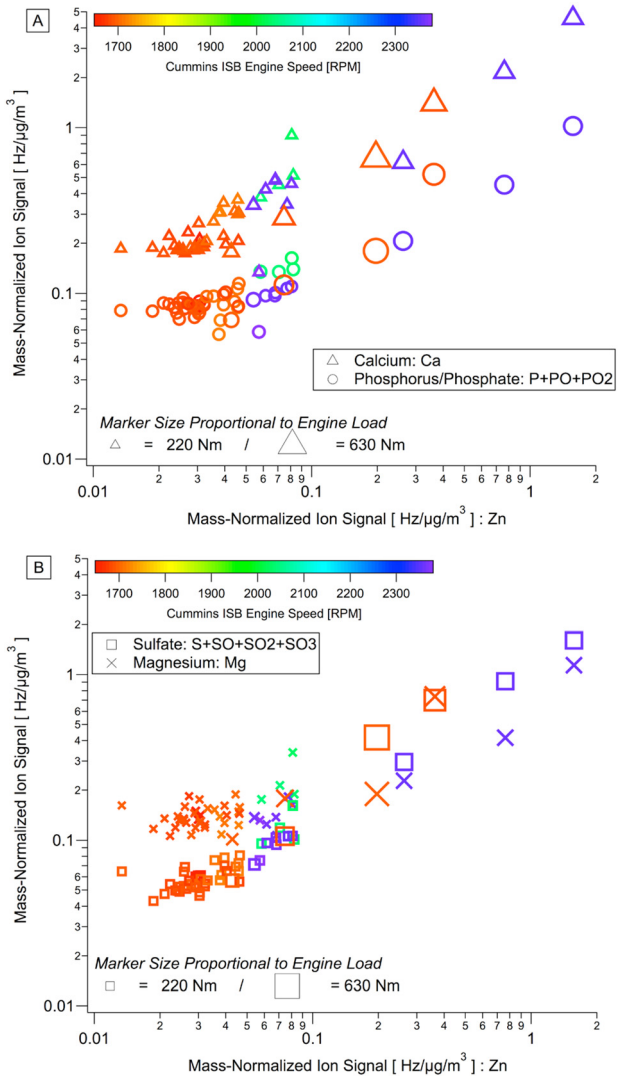

Fig. 8 (*a*) SP-AMS measured calcium and phosphorus/phosphate and (*b*) sulfate and magnesium as a function of zinc. All ion signals are normalized to the SMPS measured mass concentration. Marker color and size indicate engine speed and load, respectively.

temperature top ring zone, may contribute to the observed differences in elemental emission rates between increasing engine load and engine speed, particularly at the high speed conditions.

Simply stated, at higher engine loads lubricant volatile losses are more important than transport losses, and vice versa when engine speed is increased. In reference to Figs. 8(*a*) and 8(*b*), as engine speed is increased and liquid transport becomes the dominant oil consumption mechanism, the differences in elemental emission rates of detergent (Ca, Zn) and anti-wear (Zn) additives is reduced, i.e., emissions correspond more closely to elemental abundance in the lubricant. On the other hand, as engine load is increased at a constant speed, and volatile losses become more important, the difference in elemental oil consumption rates for calcium and magnesium relative to zinc, would be expected to increase. While this explanation appears plausible, the current data set exhibits significant variability, particularly for the high load conditions, so a definitive conclusion is not possible with the current dataset. Future studies will explore these questions in further detail.

The results shown in Figs. 8(*a*) and 8(*b*) begin to demonstrate the utility of the SP-AMS technique to provide in situ measurements to characterize engine-out emissions, but also raise a number of important questions. Relative changes in the ion signal intensities for each individual species are meaningful, but require additional analysis and validation to draw concrete conclusions regarding quantitative differences in elemental emission rates. Future characterization experiments will incorporate species-specific ionization efficiency curves that convert the measured ion signals to mass loadings for each ash species detected.

The chemical information obtained with the SP-AMS extends beyond the measurement of ions signals from lubricant-derived species. Figure 9 presents average mass spectra (displaying amu 10–100) acquired during the high-speed, high-load engine condition (2450 rpm, 630 Nm).

The upper panel in Fig. 9 shows the mass spectrum of all measured ions. This spectrum is dominated by hydrocarbon (C_xH_y colored green) and black carbon (C_x colored black) ion fragments. Note that the integrated ion signals plotted on the vertical axis of Fig. 9(*a*) extend to approximately14,000 Hz. The lower panel (Fig. 9(*b*)) displays the same mass spectrum with the hydrocarbon and black carbon fragments removed. The integrated ion axis is approximately 600 Hz and ion fragments attributed to some of the trace elements measured with the SP-AMS are shown. Figures 9(*a*) and 9(*b*) illustrate the rich nature of the SP-AMS data set especially for the detection of trace species in the sampled particulate matter.

3.5.3 Fuel-Derived Elemental Emissions. Additional trace elements in diesel fuels, such as potassium and sodium have the

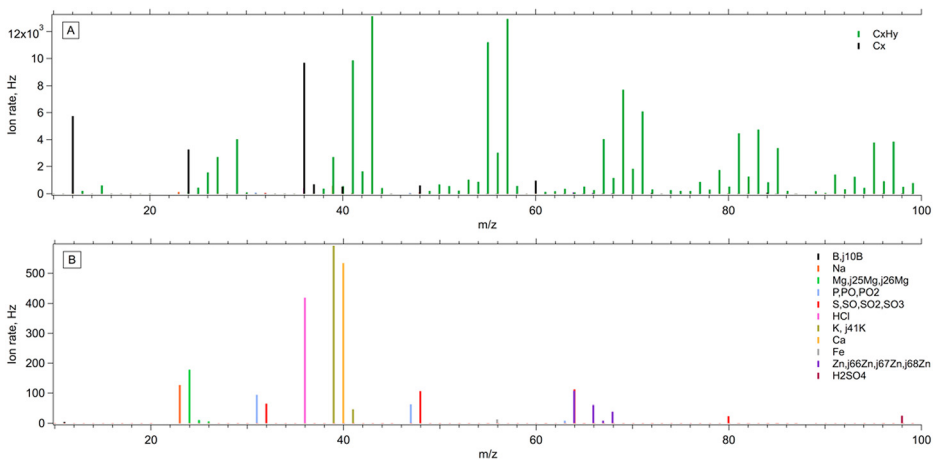

Fig. 9 Average mass spectrum measured during high speed/high load engine operation. The upper panel (*a*) plots all ion signals and is dominated by hydrocarbon fragments (C_xH_y, green) and black carbon (C_x, black). The lower panel (*b*) displays ion fragments associated with trace elements from the CJ-4, fuel, and engine wear.

potential to contribute to the accumulation of ash within the DPF or interact with the filter substrate, particularly at high levels. In some cases, biofuels may contain elevated sodium and potassium levels, which has prompted additional interest to quantify these emissions rates. In Table 4, the elemental composition of ULSD shows values for K < 2690 ppb and Na < 2010 ppb, which were below the detection limits of the inductively-coupled plasma (ICP) analysis. SP-AMS measurements of potassium and sodium are shown in Fig. 10 across the range of engine speed and load conditions tested.

Trends in potassium and sodium ion signal intensities with engine speed and load are similar to the trends observed for the lubricant-derived trace element emissions in Figs. 8(*a*) and 8(*b*). In general, significant levels of sodium or potassium are not generally found in DPF ash for engines operated with conventional ultra-low sulfur diesel. This indicates that these species may be efficiently removed from the DPF during regeneration. Additional work will further develop calibrations to quantify the magnitude of the emissions reported in Fig. 10 and track the potassium and sodium signal levels downstream of the DPF during regeneration.

3.5.4 Engine-Wear Emissions. Engine wear metals and exhaust system corrosion particles can also contribute to DPF ash. The contribution of these elements to the total ash found in the DPF is generally much less than that of the lubricant-derived components. During the course of the SP-AMS testing with the engine emissions, several engine wear-related elements were also detected in the PM, most notably lead and iron. The mass-normalized ion intensities are also presented in Fig. 11 as a function of engine-out zinc emissions.

The potential to provide in situ measurements of engine wear-related elements further highlights the utility of the SP-AMS method for additional studies outside the scope of this work.

3.5.5 Acidic Particle Emissions. The utility of the SP-AMS measurements lies in the fact that the instrument continuously samples the full mass spectrum as a function of time. Capturing the full mass spectrum enables additional analysis for a wide range of exhaust species long after the measurements were initially conducted. Figure 12 presents a further example, showing the mass normalized ion signal for particle-phase sulfuric and hydrochloric acid emissions.

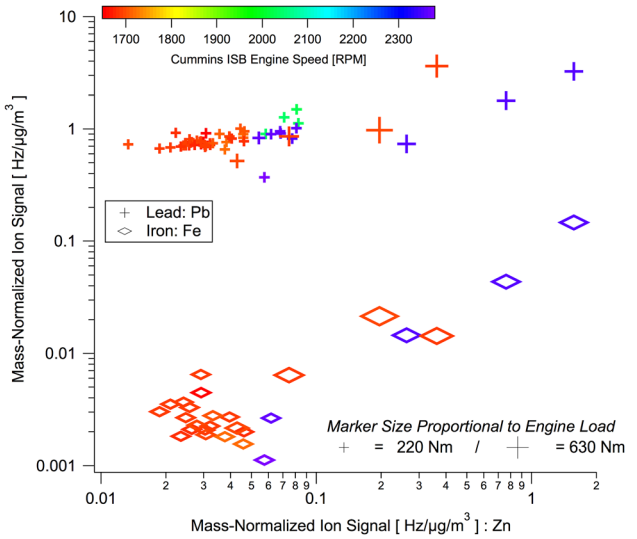

Fig. 11 SP-AMS measurements of lead and iron as a function of zinc across all engine speed and load conditions studied. All ion signals are normalized to the SMPS measured mass concentration. Marker color and size indicate engine speed and load respectively.

4 Conclusions

Trace element ash characterization studies were carried out using the SP-AMS, a real-time mass spectrometric technique for physical and chemical characterization of exhaust PM. Validation studies using an accelerated ash loading system, allowing for careful control of oil consumption, showed trace element emissions of boron, magnesium, sulfur/sulfate, phosphorus/phosphate, calcium and zinc were readily detected and positively identified, in real time, by the SP-AMS instrument. Results show increasing trace element ion signal intensities as a function of CJ-4 oil injection. Furthermore, the SP-AMS ion signal intensities scaled linearly with total particle mass during controlled calibration experiments using the accelerated ash loading system. This dataset lays the groundwork for future PM-characterization studies with the SP-

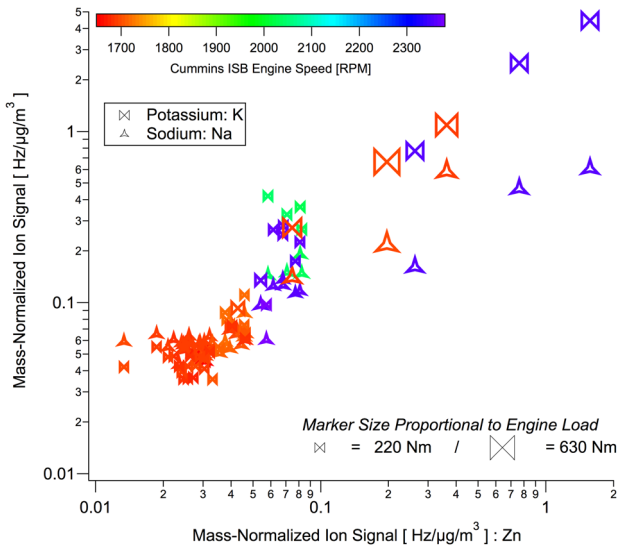

Fig. 10 SP-AMS measurements of potassium and sodium as a function of zinc across all engine speed and load conditions studied. All ion signals are normalized to the SMPS measured mass concentration. Marker color and size indicate engine speed and load respectively.

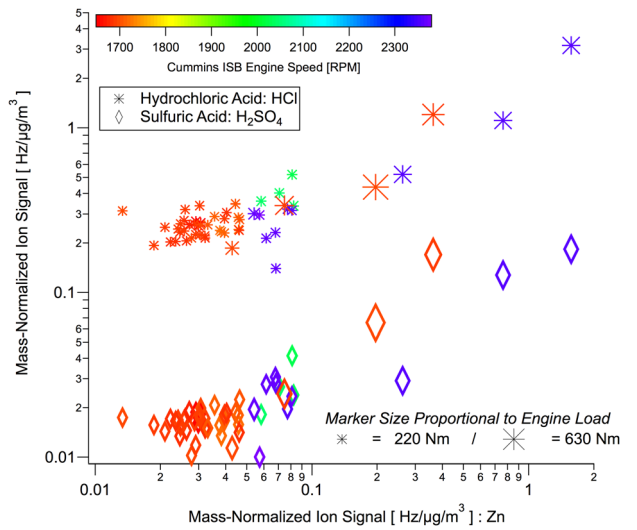

Fig. 12 SP-AMS measurements of hydrochloric acid and sulfuric acid as a function of zinc across all engine speed and load conditions studied. All ion signals are normalized to the SMPS measured mass concentration. Marker color and size indicate engine speed and load respectively.

AMS moving toward species-specific ionization efficiency curves and quantification of trace element emission factors in real-time.

Preliminary engine exhaust characterization studies were also completed with a Cummins ISB medium-duty diesel engine operated across a range of engine speed and load conditions. Lubricant-derived ash emissions were measured with the SP-AMS and trace element ion signal intensities were observed to increase during engine operating conditions of increasing bulk oil consumption, in particular high-load conditions. Differences in oil consumption mechanisms, specifically volatile and liquid losses, and differences in individual additive volatilities are believed to be the primary contributors to the observed differences in elemental emissions rates for calcium and magnesium, relative to zinc, measured during the engine speed and load sweeps.

The utility of the SP-AMS measurement technique was further demonstrated to monitor engine-wear metal emissions (lead and iron), additional trace elements (sodium and potassium) and acidic emissions (hydrochloric and sulfuric acid). This work, one of the first of its kind, demonstrates significant potential for the real-time characterization and measurement of a wide range of engine-out trace elements in the particle phase with a thermal desorption/electron impact ionization method. Future work will develop calibrations and expand the existing data set to provide a quantitative measure of the trace element emissions presented here. Advanced instrument systems, such as the SP-AMS, provide a powerful tool to enable measurements of engine- and tailpipe-out emissions and their constituents at the extremely low-levels required to keep pace with modern emissions regulations.

Acknowledgment

This publication was made possible by USEPA Grant No. RD834560. Its contents are solely the responsibility of the grantee and do not necessarily represent the official views of the USEPA. Furthermore, USEPA does not endorse the purchase of any commercial products or services mentioned in the publication. The SP-AMS instrument was developed with DOE Contract No. DE-FG02-07ER84890 SBIR, NASA Contract No. NNX10CA32C SBIR, and NOAA Contract No. NA09OAR4310125 to Aerodyne Research, Inc. The authors thank Drs. Richard Miake-Lye, Mike Timko, and Zhenhong Yu at Aerodyne Research for allowing the use of their SMPS system and Dr. Andy Lambe and Professor Paul Davidovits at Boston College for the use of their dilution plenum during the study and Dr. John Storey at Oak Ridge National Laboratory for helpful discussions. ESC is supported with a Camille and Henry Dreyfus Foundation environmental chemistry postdoctoral fellowship.

This work is supported by the MIT Consortium to Optimize Lubricant and Diesel Engines for Robust Emission Aftertreatment Systems. Sponsorship from the following participants of the Consortium made this work possible: Caterpillar, Chevron/Oronite, Cummins, Detroit Diesel, Infineum, Komatsu, NGK, Süd-Chemie, the U.S. Department of Energy Office of Energy Efficiency and Renewable Energy: Oak Ridge National Laboratory, and Valvoline. The authors are grateful to these participants for their support.

Nomenclature

AMS = aerosol mass spectrometer
DAQ = data acquisition
DMA = differential mobility analyzer
DPF = diesel particulate filter
EI = electron impact ionization
HR-TOFMS = high resolution time-of-flight mass spectrometer
ICP = inductively-coupled plasma
MS = mass spectrometer
PM = particulate matter
PTOF = particle time-of-flight
SP-AMS = soot particle aerosol mass spectrometer
SMPS = scanning mobility particle sizer
ULSD = ultra-low sulfur diesel
ZDDP = zinc dialkyldithiophosphates

Appendix A: Laboratory Appratus for Ash-Characterization Studies

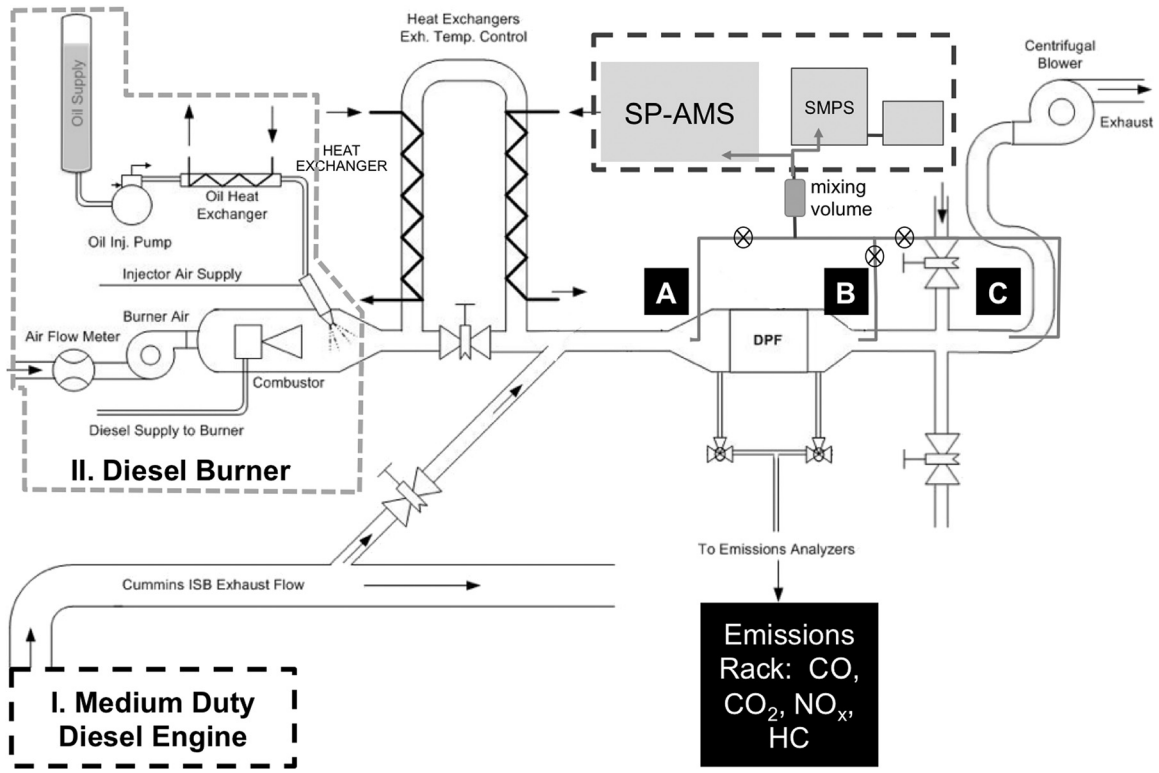

Fig. A1 Configuration of accelerated ash loading system and Cummins ISB exhaust sampling apparatus. Measurements discussed in this work were all taken from sampling position 'A' located upstream of the DPF.

References

[1] Konstandopoulos, A., Kostoglou, M., Skaperdas, E., Papaioannou, E., Zarvalis, D., and Klaopoulou, E., 2000, "Fundamental Studies of Diesel Particulate Filters: Transient Loading, Regeneration and Aging," SAE Paper No. 2000-01-1016.

[2] Givens, W., Buck, W., Jackson, A., Klador, A., Hertzberg, A., Moehrmann, W., Mueller-Lunz, S., Pelz, N., and Wenniger, G., 2003, "Lube Formulation Effects on Transfer of Elements to Exhaust After-Treatment System Components," SAE Paper No. 2003-01- 3109.

[3] Sappok, A., and Wong, V., 2007, "Detailed Chemical and Physical Characterization of Ash Species in Diesel Exhaust Entering Aftertreatment Systems," SAE Paper No. 2007-01-0318.

[4] Mayer, A., Anrea, U., Czerwinski, J., and Mooney, J., 2010, "Metal-Oxide Particles in Combustion Engine Exhaust," SAE Paper No. 2010-01-0792.

[5] Maricq, M., 2007, "Chemical Characterization of Particulate Emissions From Diesel Engines: A Review," Aerosol Sci., **38**, pp. 1079–1118.

[6] Murphy, D. M., 2007, "The Design of Single Particle Laser Mass Spectrometers," Mass Spectrom. Rev., **26**, pp. 150–165.

[7] Canagaratna, M. R., Jayne, J. T., Jimenez, J. L., Allan, J. D., Alfarra, M. R., Zhang, Q., Onasch, T. B., Drewnick, F., Coe, H., Middlebrook, A., Delia, A., Williams, L. R., Trimborn, A. M., Northway, M. J., DeCarlo, P. F., Kolb, C. E., Davidovits, P., and Worsnop, D. R., 2007, "Chemical and Microphysical Characterization of Ambient Aerosols with the Aerodyne Aerosol Mass Spectrometer," Mass Spectrom. Rev., **26**, pp. 185–222.

[8] Toner, S. M., Sodeman, D. A., and Prather, K. A., 2006, "Single Particle Characterization of Ultrafine and Accumulation Mode Particles From Heavy Duty Diesel Vehicles Using Aerosol Time-Of-Flight Mass Spectrometry," Environ. Sci. Technol., **40**, pp. 3912–3921.

[9] Spencer, M. T., Schields, L. G., Sodeman, D. A., Toner, S. M., and Prather, K. A., 2006, "Comparison of Oil and Fuel Particle Chemical Signatures With Particle Emissions From Heavy and Light Duty Vehicles," Atmos. Environ., **40**, pp. 5224–5235.

[10] Okada, S., Kweon, C., Stetter, J. C., Foster, D. E., Shafer, M. M., Christensen, C. G., Schauer, J. J., Schmidt, A. M., Silverberg, A. M., and Gross, D. S., 2003, "Measurement of Trace Metal Composition in Diesel Engine Particulate and its Potential for Determining Oil Consumption," SAE Paper No. 2003-01-0076.

[11] Jayne, J. T., Leard, D. C., Zhang, X. F., Davidovits, P., Smith, K. A., Kolb, C. E., and Worsnop, D. R., 2000, "Development of an Aerosol Mass Spectrometer for Size and Composition Analysis of Submicron Particles," Aerosol Sci. Technol. **33**, pp. 49–70.

[12] DeCarlo, P. F., Kimmel, J., Trimborn, A., Northway, M., Jayne, J. T., Aiken, A., Gonin, M., Fuhrer, K., Horvath, T., Docherty, K., Worsnop, D. R., and Jimenez, J. L., 2006, "Field-Deployable, High-Resolution, Time-Of-Flight Aerosol Mass Spectrometer," Anal. Chem, **78**, pp. 8281–8289.

[13] Onasch, T. B., Trimborn, A., Fortner, E. C., Jayne, J. T., Williams, L., Kok, G., Worsnop, D. R., and Davidivots, P., "Soot Particle Aerosol Mass Spectrometer (SP-AMS) - Instrument Development and Initial Applications" Aerosol Sci. Technol. (to be published).

[14] Sappok, A., and Wong, V., 2011, "Lubricant-Derived Ash Properties and Their Effects on Diesel Particulate Filter Pressure Drop Performance," J. Eng. Gas Turbines Power, **133**(3), 032805.

[15] Sappok, A., Beauboeuf, D., and Wong, V., 2008, "A Novel Accelerated Aging System to Study Lubricant Additive Effects on Diesel Aftertreatment System Degradation," SAE Paper No. 2008-01-1549.

[16] Sappok, A., Santiago, M., Vianna, T., and Wong, V., 2009, "Characteristics and Effects of Ash Accumulation on Diesel Particulate Filter Performance: Rapidly Aged and Field Aged Results," SAE Paper No. 2009-01-1086.

[17] Scientific Instrument Services, 2010, "Exact Masses of the Elements and Isotropic Abundances," http://www.sisweb.com/referenc/source/exactmas.htm.

[18] Liu, P. S. K., Deng, R., Smith, K. A., Williams, L. R., Jayne, J. T., Canagaratna, M. R., Moore, K., Onasch, T. B., Worsnop, D. R., and Deshler, T., 2007, "Transmission Efficiency of an Aerodynamic Focusing Lens System: Comparison of Model Calculations and Laboratory Measurements for the Aerodyne Aerosol Mass Spectrometer," Aerosol Sci. Technol., **41**, pp. 721–733.

[19] Jimenez, J. L., Jayne, J. T., Shi, Q., Kolb, C. E., Worsnop, D. R., Yourshaw, I., Seinfeld, J. H., Flagan, R. C., Zhang, X., Smith, K. A., Morris, J. W., and Davidovits, P., 2003, "Ambient Aerosol Sampling Using the Aerodyne Aerosol Mass Spectrometer," J. Geophys. Res., **108**(D7), pp. 8425.

[20] Froelund, K., 1999, "Real-Time Steady-State Oil Consumption Measurement on Commercial SI-Engine," SAE Paper No. 1999-0-3461.

[21] Froelund, K., Menezes, L., Johnson, H., and Rein, W., 2001, "Real-Time Transient and Steady-State Measurement of Oil Consumption for Several Production SI-Engines," SAE Paper No. 2001-01-1902.

[22] Watson, S., 2010, "Lubricant-Derived Ash : In-Engine Sources and Opportunities for Reduction," Ph.D. thesis, Massachusetts Institute of Technology, Cambridge, MA.

[23] Yilmaz, E., Tian, T., Wong, V., and Heywood, J., 2004, "The Contribution of Different Oil Consumption Sources to Total Oil Consumption in a Spark Ignition Engine," SAE Paper No. 2004-01-2909.